STM JOURNALS

Journal of
Polymer & Composites

https://journals.stmjournals.com/jopc

ISSN: 2321-2810 (Online)
ISSN: 2321-8525 (Print)
Volume 14, Special Issue 4, 2026
January–December
DOI (Journal): 10.37591/JoPC

Research JoPC

The Effect of Welding Parameters and Tool Geometry on Mechanical Properties of RZ5-10 wt% TiC FSW Joint

Deepak Mehra[1], J. G. Nayak[2], Prashant Sunagar[2], D. S. Sawake[3], V. B. Patil[3], Rahul T. Pardeshi[2,*]

Abstract

Friction Stir Welding (FSW) of metal matrix composite (MMC) provides the grain refinement and reinforcement redistribution of the composite used for wide application in aerospace and structural. This wide application needs development of best-suited joining process for MMC which is complicated to unite by the traditional welding process. The paper observed the consequence of the welding parameters and tools' geometry on the mechanical properties of the friction stir butt welded in-situ RZ5-10 wt% TiC composite. The flame-hardened tool steel is utilized as a material for the tool. The welding has been done using different welding speeds (931, 1216 mm/min), Tool speed (30, 40 rpm) and shoulder diameter of the tool (17, 19 and 21 mm). The grain refinement of the RZ5-10 wt% TiC composite and matrix alloy observed in weld stir zone. It is due to grain size decrease in RZ5-10 wt% TiC composite. The microstructural investigations have been analyzed by means of scanning electron microscopes. The hardness tests on Vickers hardness tester showed fairly increased in mean hardness of the welded composites according to the designated parameters. The UTS of the welded composite is increased in comparison to RZ5-10 wt% TiC composite. The predictive model has also been developed based on the full factorial design to evaluate the welding parameters. Further, the multi-response technique was utilized to optimize the welding parameters. The observed 0.39% error revealed the competence of the model in the optimality test.

Keywords: FSW, magnesium alloy, mechanical properties, tool speed, welding speed

INTRODUCTION

Friction stir welding is latest joining method introduced in 1991 for structural, aerospace, etc. application part [1]. The FSW is designed for parts which are not welded by conventional welding processes [2, 3]. The FSW has no liquid state in weld pool like other conventional welding processes. So, the temperature is very less compared to others, produce the sound defect-free weld with lower residual stresses [4, 5]. It is also used to weld soft structural alloy like magnesium and aluminum. However, some geometrical parameters of FSW – like tool, force, tilted angle – contributed to weld flaw [6].

Recently, Mg alloy considered due to their Machinability, high damping capability, low density, and electromagnetic shielding. Many authors reported that AZ31 magnesium alloy successfully joined by FSW [7, 8]. Recently, researchers have reported FSW of Mg alloys like AZ series, heat-resistant Mg alloys, and AM series [9, 10]. Schubert et al. [11] reported Al and Mg

***Author for Correspondence**
Rahul T. Pardeshi
E-mail id: rahul.pardeshi@sitrc.org

[1]Associate Professor, Department of Mechanical Engineering, National Institute of Technical Teachers' Training and Research, Kolkata, West Bengal, India
[2]Associate Professor, Department of Civil Engineering, Sandip Institute of Technology and Research Centre, Nashik, Maharashtra, India
[3]Assistant Professor, Department of Civil Engineering, Sandip Institute of Technology and Research Centre, Nashik, Maharashtra, India

Received Date: June 16, 2026
Accepted Date: July 04, 2026
Published Date: July 29, 2026

Citation: Deepak Mehra, J. G. Nayak, Prashant Sunagar, D. S. Sawake, V. B. Patil, Rahul T. Pardeshi. The Effect of Welding Parameters and Tool Geometry on Mechanical Properties of RZ5-10 wt% TiC FSW Joint. Journal of Polymer & Composites. 2026; 14(Special Issue 4): S81–S94p.

alloy is the best possible material for future proposals in the automotive and aerospace sectors. Nowadays, Mg alloys are welded using metal arc/inert gas (MIG) welding and tungsten arc/inert gas (TIG) welding [12]. The problems experienced using these welding techniques change in metallurgical structure experiencing the high melting point and high residual stresses. The high melting zone and porosity problem were also seen in laser welded Mg alloys [13].

Nakata et al. [14] reported friction stir (FS) welds of thixomolded AZ91D without defect. Park et al. [15] reported microstructure evolution of FSW homogenized thixomlded AZ91D and found enhanced mechanical properties. Lee et al. [16] investigated that reduced welding speed and elevated rotating speed of the FSW tool exhibits defect free sound weld in AZ31B-H24. Esparza et al. [17] also reported sound AM60 thixomolded plates joined using FSW at elevated tool speed of 2000 rpm and a low welding speed of 120 mm/min. Don-Hyun Choi et al. [18] inspected the micro-structural as well as mechanical properties of AZ31with CaO alloys FSW weld at tool speed of 1600 rpm and welding speed of 80 mm per minute, respectively. They reported that very fine grain presented in stir zone due to dynamic re-crystallization. Further, they found an increase in hardness of stir zone due to Al2Ca intermetallic compound. Similarly, U.F.H.R. Suhuddin et al. [19] studied grain structure development of AZ31 Mg alloy during FSW and discovered that tool shoulder considerably impacts the material flow in top half part of the weld. The material flow in lower part was due to the pin. Datong Zhang et al. [20] reported microstructure development of heat-resistant Mg alloy owing to FSW. They state that microstructure of the parent material is substitute with fine Mg grain and intermetallic Al2Ca causes enhancement of micro-hardness in stirring zone assesses to the matrix material. Nagasawa et al. [21] investigated mechanical properties, like toughness, hardness, and tensile of sound welded AZ31 alloy, and found same properties of FWS weld as of parent material.

N. Afrin et al. [22] delved into the tensile properties of FSW AZ31alloy. They reported that tensile strength improved by rising the welding speed from 500 to 1000 rpm. Also, fracture surfaces showed that dimple and cleavage characteristic of weld. Many researchers have been reported that grain structure refined through severe plastic deformation and continuous recrystallization during friction stir processing [23–25]. Won-Bae Lee et al. [26] investigated the joint properties of FSW AZ91 alloy. They reported that optimum welding parameters of AZ91 weld were 41–187 mm/min welding speed and 115–131 rad/s tool rotational speed. The mechanical properties of weld also increased in stir zone due to grain refinement using optimum welding parameters. Elangovan et al. [27] observed the effect of probe & traverse speed of AA-2219 alloy in FSP zone. They used five different tools probes and three traverse speeds for the fabrication of joints. The tool probe which has square shape has been discovered appropriate for fabrication of sound defect free joint at the traverse speed of 0.76 mm per second.

M. Azizieh et al. [28] reported that effect of probe profile & traverse speed of AZ31/Al2O3 nanocomposite on hardness and microstructure fabricated using FSP. They stated that 1000 and 1200 rpm rotational speed was very close to the experimental and calculated hardness of composite. In the friction stir processing the TiC particles are subjected to severe plastic deformation in the Mg-alloy. The author reported the change in grain size and morphology during friction stir welding. M. Balakrishnan et al. [29] reported friction stir processing of AZ31/TiC Mg composite. The composite was synthesized using tool speed and welding speed of 1200 rpm and 40 mm/min, respectively, at 10 kN vertical loads. They found the uniform distribution of TiC particles in AZ31 Mg alloy. G. Faraji et al. [30] reported friction stir processing of Al2O3/AZ91 nanocomposite. They found that the optimum values of welding parameters were 80 mm/min for sound defect free welded composite and 900 rpm rotational speed. The higher grain refinement and hardness were achieved using nano Al2O3 in AZ91 Mg alloy. D. Khayyamin et al. [31] studied the consequence of welding parameters of FSP fabricated AZ91/SiO2 on its microstructure. They used constant rotational-speed 1250 rpm and 3-different welding speed (63, 40 and 20 mm per min) for composite. The authors reported that the size of grain decreases as traverse speed increases in the nugget zone. Similarly, hardness and UTS also increases as grain size decreases. P. Asadi et al. [32] produced AZ91/SiC ultra-fined nanocomposite using friction stir processing. They stated that the size of grain increases by improving tool speed and reduced by growing traverse speed. Also, hardness increased in stir zone.

Regarding rare earth contains magnesium alloys and its composite, which are being used to the aerospace application, no investigation has been reported on FSW till now. In the present study, RZ5-10 wt% TiC composite was synthesized by the SHS technique and subsequently joined using FSW. The welded specimens were sectioned perpendicular to the weld line to evaluate the effects of tool geometry and process parameters on the mechanical behavior and microstructural evolution of the welded joints. Further, the full factorial design, predictive model was utilized to assess optimum parameters of welded composites. The results obtained from the model consistent well within the range of the experimental results.

DETAILS OF EXPERIMENT

Preparation of Material

In the current study, the in-situ RZ5/10%TiC composites are prepared using Self-propagating high-temperature synthesis technique. The weighted quantity of RZ5 magnesium alloy was melted at 750°C using the furnace. The titanium melted at 1650°C in another furnace then temperature rose to 1850°C. The preheated carbon that introduce in the titanium melt, and mechanical stirring was applied for 15 minutes. Subsequently, the molten titanium and carbon were transferred into the molten RZ5 magnesium alloy. The mechanical stirring applied for 5 minutes to allow diffusion of titanium and carbon melt in the molten matrix which was enough for the formation of TiC in the matrix. At last, the cast ingots were molded in the permanent mold after removed impurities from molten metal [33, 34].

Further, the cast welded specimens were sectioned to the dimension of 200 × 100 × 6 mm using the powered hacksaw. The welded plates were further machined to 100 x 50 mm to prepare butt size using shaper machine.

Details of FSW

The FSW composite samples prepared using vertical milling machine 7.5 HP as revealed in Figure 1. The three different tools used for welding state shoulder diameter 17 mm, 19 mm, and 21 mm with 1 mm anticlockwise thread pitch. The flame-hardened probes of tool followed by oil quench are used to protect adhering of the TiC particle. The tool material composition is Fe = 51%, C = 0.25%, Cr = 25.1%, Ni = 20%, Mn = 2% and remaining P, S, and Si.

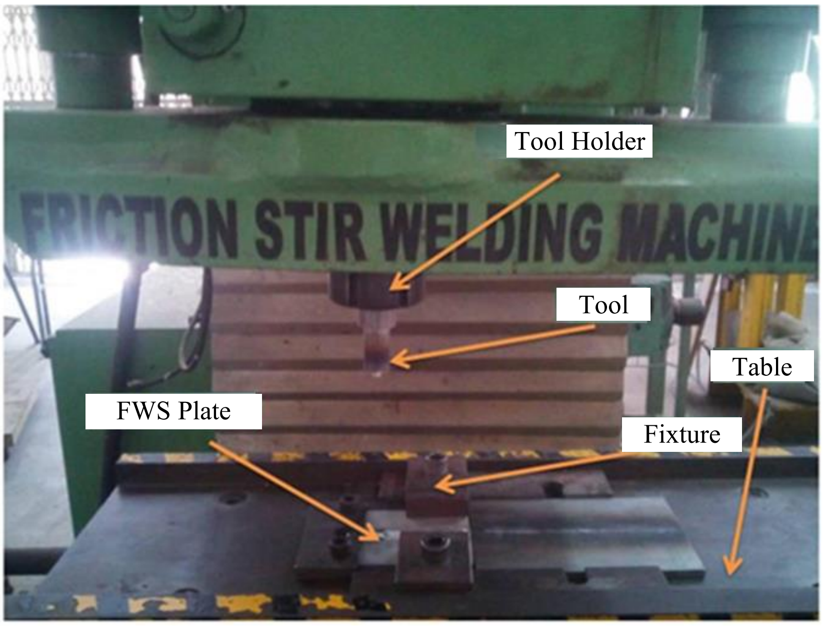

Figure 1. Arrangement of the friction stir welding process.

The tool was fixed with suitable collate and mounted on the arbor of the vertical milling machine. The FSW plates were clamped to the fixture on the machine table without root gap.

The center of both plates adjusted with reference to the tool before the start of welding. The dimensions of tool shoulders were selected according to the previous study [28–32]. Figure 2 shows the dimensions of three different used tools. The welding parameters were selected based on trial experimental runs. The best appropriate welding parameters fixed are the vertical load of 6 kN, welding speed (WS) of 30 as well as 40 mm/min and tool speed (TS) of 931 and 1216 rpm. These selected parameters produced sound defect free welded joints. The sound welded joint was not achieved below and above the selected parameters. Hence, 12 experimental runs were planned using welding parameters, such as tool speeds (931 rpm and 1216 rpm), flat surface of tool shoulder with Ø17 (Tool Type (TT) 1), Ø19 (Tool Type 2) Ø21 (Tool Type 1) mm diameter and WS (30 and 40 mm per minute) based on full factorial design. Table 1 provided levels of the FSW welding parameters. Further, the statistical model was formulated to predict the impact of welding constraints on the response (UTS) using Minitab software. Table 2 demonstrates the experimental value of response UTS based on selected welding parameters. To correlate response with welding parameters, the regression equation was developed. The validation test also performed to ensure the competence of the developed regression equations. At last, multi-response optimization was performed to optimize joint characteristics of the composite. The image of FSW plates of welded composite as shown in Figure 3. Figure 3 [(1) and (4)] welded at constant 931 rpm tool speed for welding speed of 30 and 40 mm per min, respectively. Similarly, Figure 3 [(2) and (5)] welded at constant 1216 rpm tool speed & welding speed of 30 as well as 40 mm/min, respectively. It is observed that sound welding with good surface finishes achieved at 1216 rpm tool speed & 30 mm/min welding speed. The entire plate shows defect-free weld with different surface finish level.

Figure 2. Tool of different shoulder diameters 17 (tool type 1), 19 (tool type 2), and 21 (tool type 3) mm.

Figure 3. Image of FSW samples.

The tensile samples were prepared from the welded composite confirming to the ASTM: E8M-04 standard as shown in Figure 4. The weld plate was 10 mm wide, 6 mm thick and had a 25 mm gauge length. The two tensile samples were tested using INSTRON tensile test machine at 10 mm/min constant head for each test & avg. reported. The samples' micro-hardness was measured at the load of 100 gm for fifteen seconds using OMNITECH micro-hardness tester.

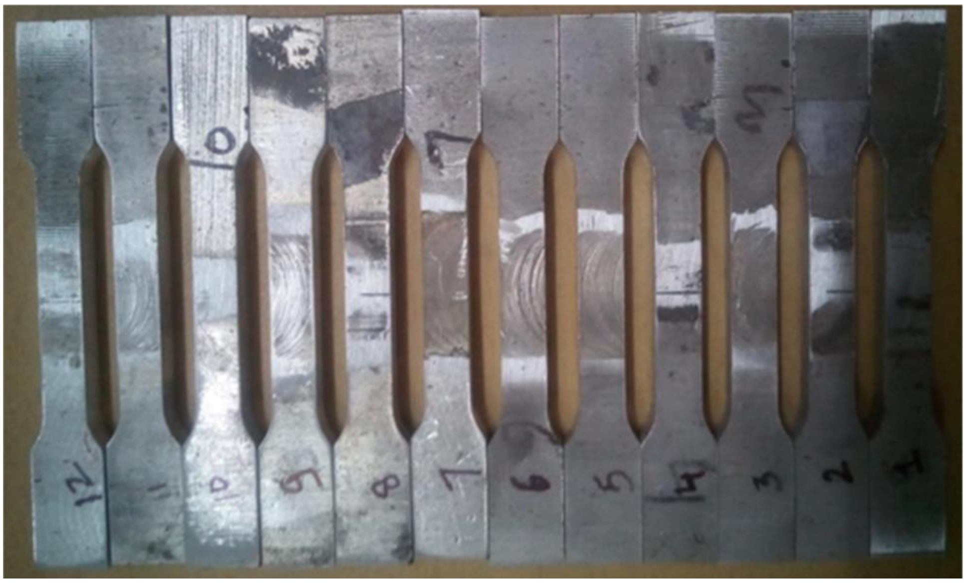

Figure 4. Image of tensile specimens.

Microstructure Analysis

The macrostructure of the FSW composite cross-section produced at a tool rotational speed of 1216 rpm and traverse (welding) speed of 30 mm/min is presented in Figure 5. The friction stir zone (FSZ) in this zone has a measured width of approximately 6 mm. The FSW sample first polish with the help of emery paper up to the 2000 grade and finally Magnesium oxide is used for fine polishing of the sample. Further, the specimen is etched by Picral reagent to reveal the temperature affect region and stir region of the weld. The stir zone appears brighter after doing the etching. Both side of the weld zone retreating side (RS) and advancing side (AS) as demonstrated in Figure 5. Figure 5(a), (b), (c) and (d) indicated the various zone of macrostructure as Stir zone, TMAZ, HAZ and the base material of composite. Figure 6 shows SEM images of the FSW welded composite at different welding parameters. Figure 6 (a), (b) and (c) shows interface of three distinct zones, i.e., SZ, HAZ and TMAZ confirming stir-zone, heat-affected-zone, and thermo-mechanically-affected-zone. Figure 6(d) and (e) shows distinct SZ and base material zone of composite, respectively. The TiC particles have been seen very coarse and fine evenly distributed in HAZ and stir zone, respectively. The TiC particle is evenly distributed due to the heat generated during stirring. The redistribution and re-crystallization of TiC particles indicated grain refinement in stir zone.

The TMAZ was found together with the SZ. The SZ of Figure 6.1, 6.2, 6.3 and 6.4 shows the grain refinement of the welded composite. Figure 6.2(d) shows very fine grain in comparison to the others shows well-defined grain refinement due to the redistribution and re-crystallization of TiC particles at 1216 rpm tool speed & 30 mm/min welding speed. The above optimum values are also derived from the model. The close agreement between the model predictions and the experimental results confirms the validity of the model.

Table 1. Welding parameters at different levels.

Parameters	Units	Levels		
		First	Second	Third
TT	–	1	2	3
TS	Rpm	931	1216	–
WS	mm/min	30	40	–

Table 2. Measured welding parameters.

S. N.	TT	TS (RPM)	WS (mm/min)	UTS (MPa)
1	1	931	30	222.27
2	1	931	40	215.78
3	1	1216	30	230.58
4	1	1216	40	223.34
5	2	931	30	221.24
6	2	931	40	212.21
7	2	1216	30	236.36
8	2	1216	40	228.57
9	3	931	30	196.85
10	3	931	40	188.39
11	3	1216	30	214.13
12	3	1216	40	207.27

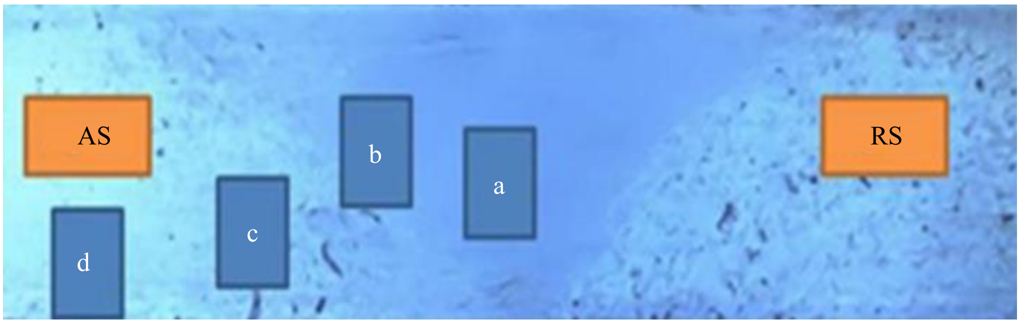

Figure 5. Macrostructure of the section of FSW composite.

ISSN: 2321-2810 (Online) ISSN: 2321-8525 (Print)

Figure N.	Interface of (a) SZ, (b) TMAZ, and (c) HAZ	(d) Stir zone	(e) Base material
6.1	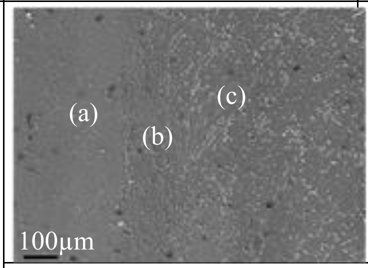	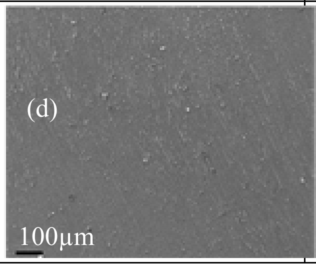	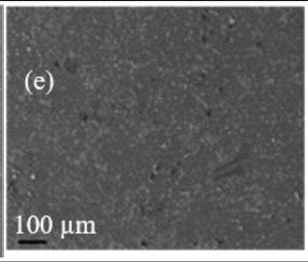
	Tool speed = 931. Welding speed = 30.		
6.2	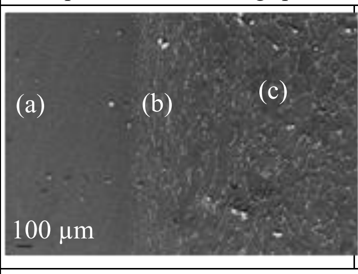	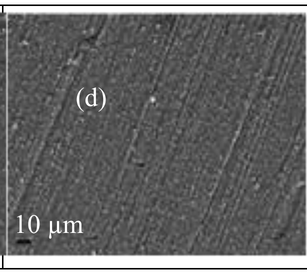	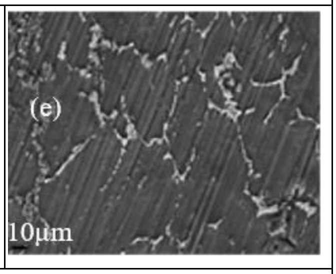
	Tool speed = 1216. Welding speed = 30.		
6.3	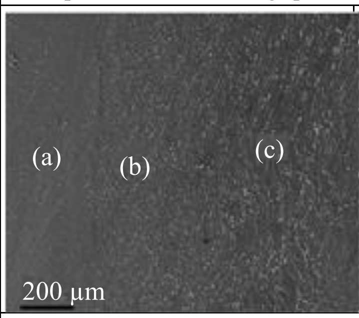	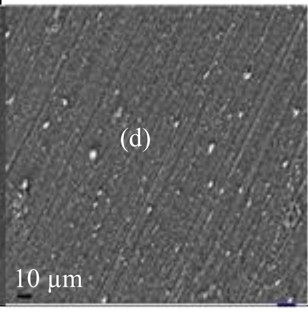	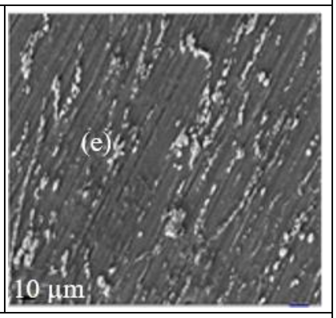
	Tool speed = 1216. Welding speed = 40.		
6.	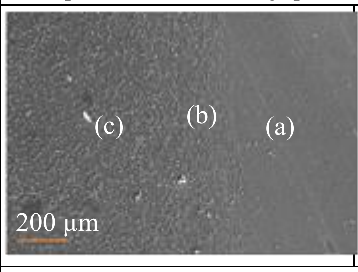	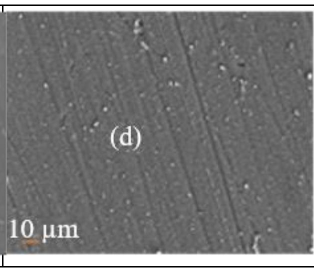	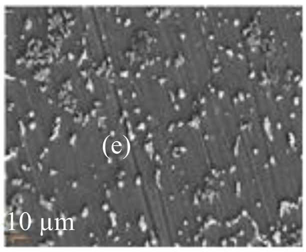
	Tool speed = 931. Welding speed = 40.		

Figure 6. Microstructure of the different zones of FSW composite.

RESULT & DISCUSSION

Effect of Welding Parameters on Mechanical Properties

The effect of welding parameters on the in-situ RZ-10 wt% TiC composite was predicted using statistical analysis in MINITAB software. The influence of these parameters on the UTS of the welded specimen was examined at three levels, as illustrated in Figure 7. From Figure 7, it can be observed that Tool 2 showing higher UTS as compared to the other two. Similarly, Tool 3 has lowest UTS. In contrast, the influence of both speeds (tool and welding) on the UTS increases linearly from 931 to 1216 rpm and decreases linearly from 30 to 40 mm per minute, respectively. This shows the consequences of TT and TS having a greater influence on UTS than welding speed. The favorable welding parameters are tool type 2, 1216 rpm and 30 mm/min based on the higher is best criteria. This also shows that tool type 2 comprises superior shoulder surface contact area which resulted in higher friction heat generation compared to the other two tool types. This results in higher UTS of the weld.

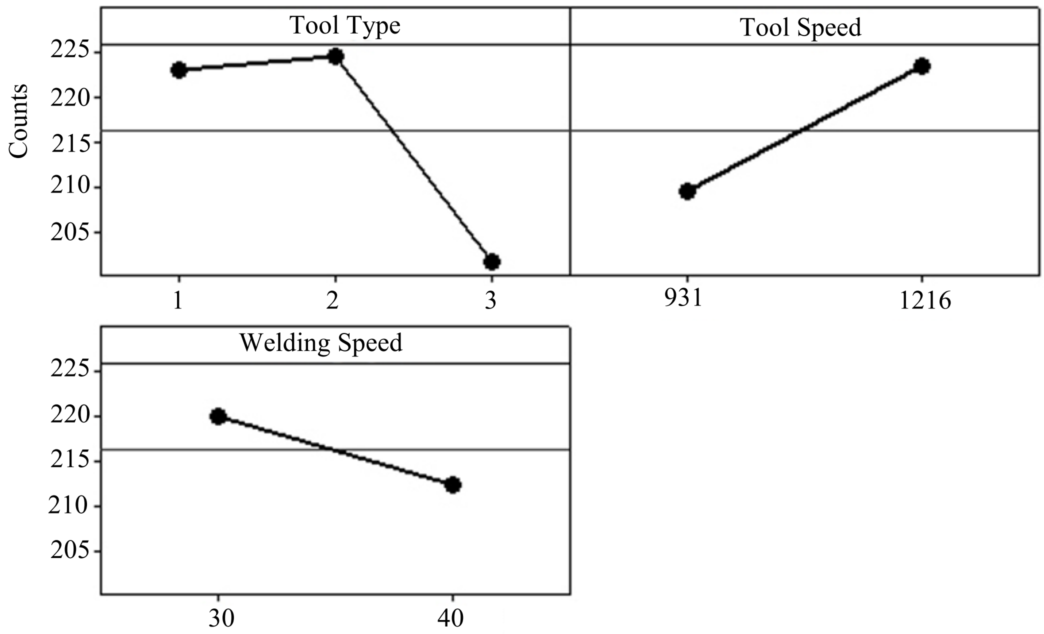

Figure 7. Main effect plot for UTS.

PREDICTIVE MODEL

The experimental values of the UTS considering three welding parameters further utilized for the analysis of variance. The regression equations (full quadratic) wear developed to correlate welding variables using MINITAB.

Table 3 presents the ANOVA findings of the UTS. The R^2 and Adj R^2 are generated using the multi-regression models. This shows the variability in the data sample. The Adj R^2 incorporates the effect of degree of freedom related to the sum of squares. In addition, Table 3 summarizes the sequential sum of squares (Seq SS), adjusted sum of squares (Adj SS), and adjusted mean squares (Adj MS). These ANOVA results are utilized to assess the significance of the welding parameters and their interaction effect on UTS.

Table 3. ANOVA for UTS.

Source	DF	Seq SS	Adj SS	Adj MS	F	P
Regression	7	2120.18	2120.18	302.883	182.01	0.000
Linear	3	1666.65	1666.65	555.550	333.84	0.000
Square	1	401.39	401.39	401.393	241.20	0.000
Interaction	3	52.14	52.14	17.380	10.44	0.023
Residual Error	4	6.66	6.66	1.664		
Total	11	2126.84				

Note: R-Sq = 99.69%, R-Sq (adj) = 99.14%.

The P value shows the probability of significance of ANOVA table. The variance ratio was used to calculate the P value. Accordingly, P <0.05 shows the significant effect of control factor on the response. The P value is less than 0.05 for regression; linear, square and interaction of control factors on UTS are significant as shown in Table 4. The value of R2 and Adj R2 were obtained as 99.69% and 99.14% for UTS, respectively. The obtained regression equation is as follows:

$$UTS = [215.79 + (20.693 * TT) + (0.0047 * TS) - (0.947 * WS) - (12.269 * TT * TT) + (0.0178 * TT * TS) - (0.0397 * TT * WS) + (0.0002 * TS * WS)]$$

where TS and TT are tool speed and type, respectively, whereas welding speed denoted using WS Table 5.

ISSN: 2321-2810 (Online) ISSN: 2321-8525 (Print)

Table 4. Measured and predicted UTS.

Predicted UTS (MPa)	Measured UTS (MPa)	% Error
222.989	222.1118	0.39

Table 5. Local solution (L.S) and global solutions (G.S) for UTS.

L.S. & G. S.	Predicted welding parameters			Predicted O/P	Composite desirability
	(TT)	(TS)	(WS)	UTS	
L.S	1.05474	933.233	30.0546	222.989	0.999695
L.S	1	1216	40	223.966	0.931012
L.S	2	1073.5	37.0863	223	1.000000
L.S	2.75214	1215.75	30.0005	222.281	0.979461
L.S	1.41597	931.001	39.9716	217.303	0.837235
L.S	2.52381	1215.52	39.8819	220.237	0.921063
L.S	2.72514	1216	30	223	1.000000
G. S	1.05474	933.233	30.0546	222.989	1.000000

Validation of the Model

The different experimental values (other than main experimental value) of control factors are used to verify the predictive model. The measured and predicted values of UTS are provided in Table 6. Table 6 also provided error% in both values. The errors are obtained from 2% to 3.60% for UTS. It shows developed regression equations successfully predict the value of UTS for friction stir joined RZ-TiC composite.

Table 6. Conformation results.

S. N.	TT	TS	WS	Measured UTS (MPa)	Predicted UTS (MPa)	Error %
1	1	600	30	206.32	211.96	2.66
2	1	1500	40	222.71	231.04	3.60
3	2	600	30	201.22	205.33	2.00
4	2	1500	40	232.46	240.03	3.15
5	3	600	30	170.26	174.17	2.24
6	3	1500	40	217.24	224.49	3.22

Optimization of the Model

The multi-response optimization approach was employed to determine the optimal welding parameters of sound welded RZ5-10 wt% TiC composite plates. The full quadratic equation is used to develop the surface plots to estimate the available responses and accordingly set the D-optimality of the response equal to 1. Figure 8 shows the 3-D surface plots for response uses three different hold values namely low, middle and high welding parameters. The curvature of the plot shows the optimality of the response. The regression equation of UTS shows the individual and interaction effect of the weld parameters.

The optimistic values of welding parameters and UTS can be determined using local and global solutions which are generated by the Minitab software. Table 5 shows the local and global solution of UTS. The composite desirability is obtained 1.00000 for the global solution. It shows the compatibility of welding parameters with the response. Table 4 shows the percentage error between measured and predicted value of UTS. Many authors suggested the joint efficiency of the in-situ composite is to be more than the base material. In these studies, the predicted UTS of the welded composite is 222.11 and the UTS of RZ5-10 wt% TiC composite is 200 MPa. This shows that the presently used optimization technique is appropriate to predict the values of response.

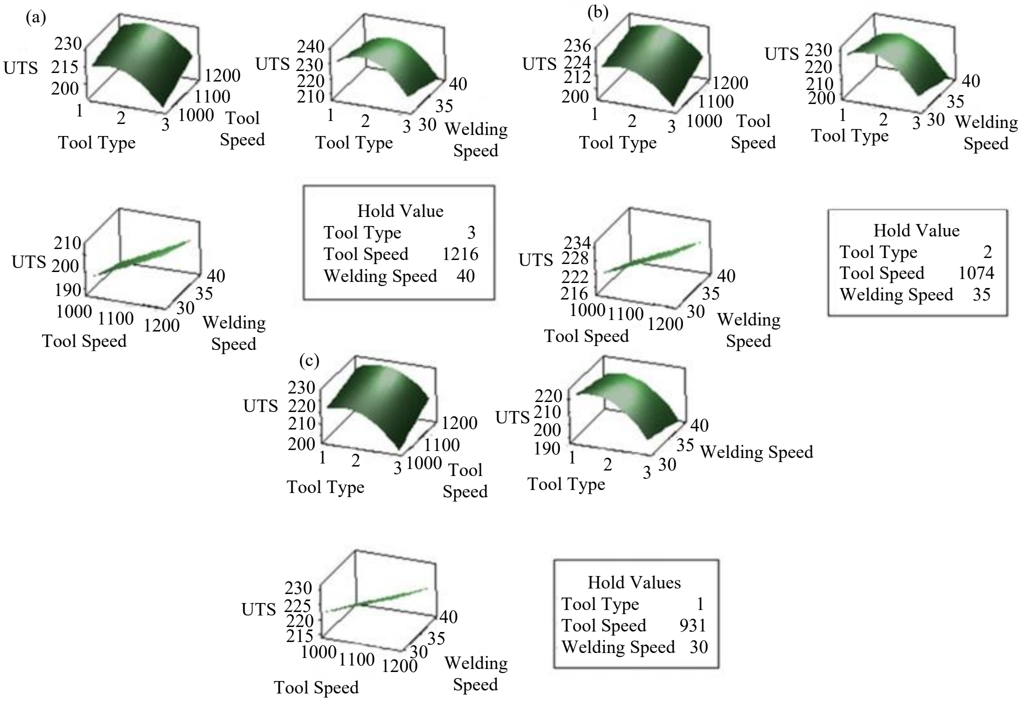

Figure 8. Response surface of UTS.

MICRO-HARDNESS

The micro-hardness profile across weld of RZ5-10 wt% TiC composite is shown in Figure 9. The average micro-hardness was measured based on the optimized parameters, i.e., TT 2, TS 1216 rpm and WS 30 mm/min. The stir zone has high hardness as shown in Figure 9. The hardness decreased towards HAZ because of the finer and more uniform grains in nugget region of the welded composite. The rise in hardness from HAZ to TMAZ can be attributed to work hardening during the welding process. Additionally, the hardness level in HAZ is lower than that of the RZ5-10 wt% TiC material [35].

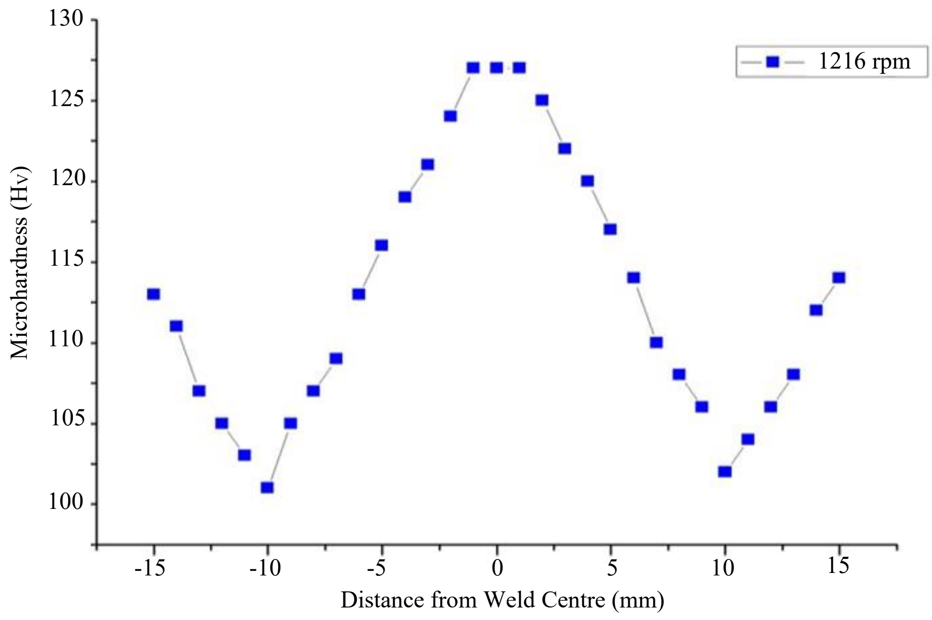

Figure 9. Micro-hardness profile of FSW weld.

Journal of Polymer & Composites
Volume 14, Special Issue 4
ISSN: 2321-2810 (Online) ISSN: 2321-8525 (Print)

FRACTOGRAPHY

The fracture surface was examined using Scanning electron microscopy as shown in Figure 10. The whole fracture mode was mixed failure which includes both brittle and ductile mode of fracture surfaces in each sample. Almost all samples failed in the HAZ zone because it is the weakest zone where the grains were columnar and elongated. Due to the elongation of grains, the concentration of stress mainly took place in these grains. Whereas weld nugget was comprised of fine equiaxed grains.

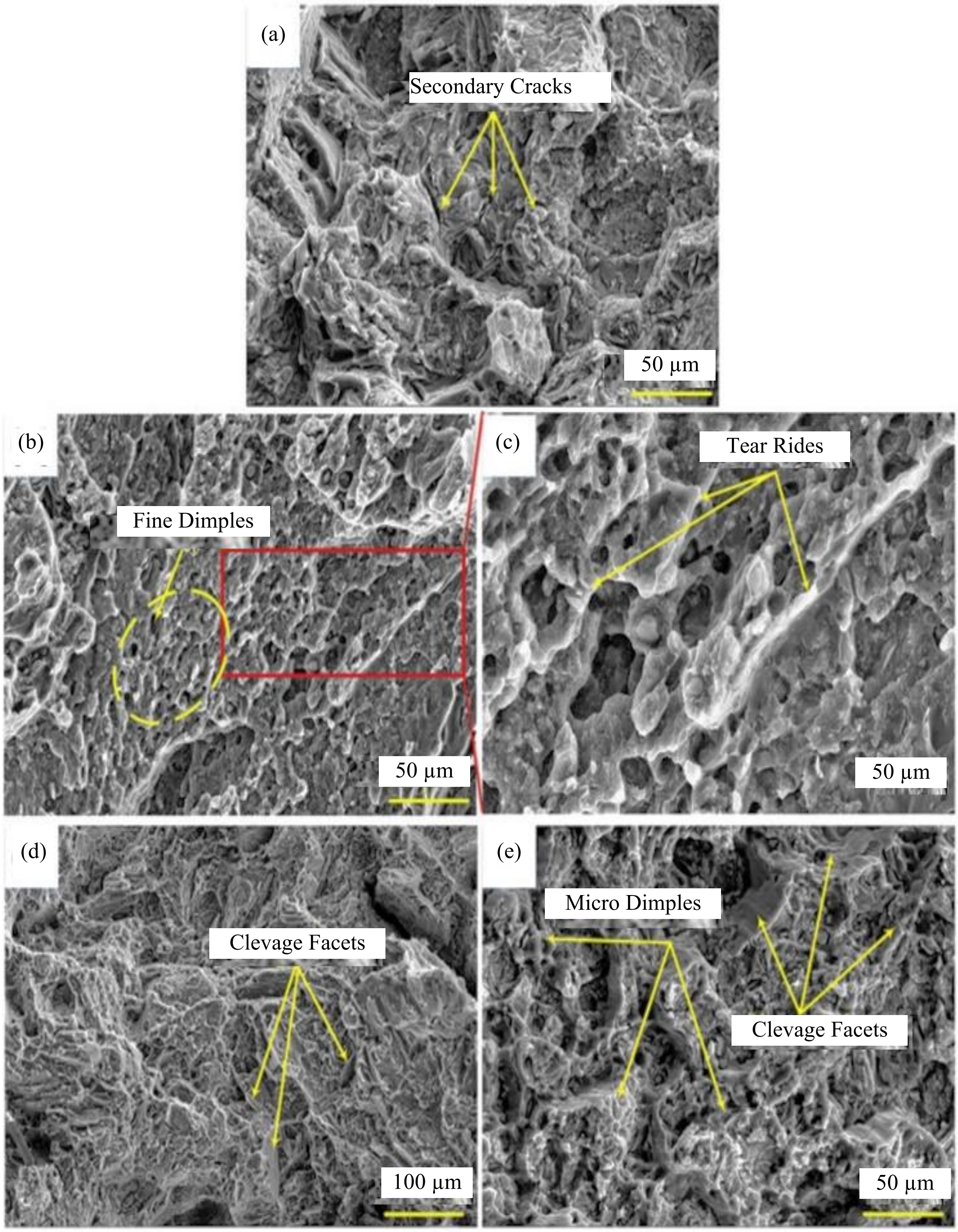

Figure 10. Fracture surface of FSW sample (a, b, c) at 931 rpm and 30 mm/min and (d, e) at 1216 rpm and 30 mm/min.

The tensile stress distribution in these grains will be uniform compared to the HAZ and TMAZ zone.

The above Figures depict the fracture surface investigated during the welding at tool speed of 931, 1216 rpm & welding speed at 30 mm/min. The fracture took place in an area between weld nugget and TMAZ zone. The TMAZ fracture side depicts almost a brittle mode of fracture which includes secondary cracks inside the matrix which is clearly shown in Figure 10(a) and (b) shows fine dimples, which was the fracture surface overlapped with the weld nugget area since it contains fine equiaxed grains, the fracture surfaces were showing fine dimples and the magnified images are showing tear ridges in Figure 10(c). These fine dimples were responsible for the ductility inside the weld zone. Figure 10(d) shows the fracture surface at similar welding speed 30 mm/min and tool speed of 1216 rpm. This fracture took place clearly within the TMAZ zone. The fracture surface mainly consists of cleavage facets due to the shearing took place between the cast dendrites. Figure 10(e) shows the magnified portion of the same fracture zone which clearly indicates the presence of a major portion of cleavage facets and micro dimples within the TMAZ zone due to the dynamic re-crystallization on Mg matrix.

CONCLUSIONS

The effect of process variables on the UTS of RZ5-10 wt% TiC MMC has been investigated. The succeeding conclusions are made based on the present findings:

- The most significant FSW parameters are tool speed 1216 rpm, welding speed 30 mm/min and tool type 2 to develop sound joints.
- The tool type 2, i.e., 19 mm shoulder diameter, tool speed 1216 rpm and welding speed 30 mm/min is preferred for UTS.
- The scanning electron micrographs of FSW sample show fairly well grain redistribution and refinement of TiC in stir zone.
- The effect of welding parameters on response was predicted satisfactorily using multiple regression models.
- The observed errors for UTS were obtained using multiple regression models.
- The optimization test shows observed errors were 0.39% for UTS.
- The highest hardness value was recorded in the SZ, while the lowest was found in the HAZ of the welded composite.

REFERENCES

1. Prater T. Friction stir welding of metal matrix composites for use in aerospace structures. Acta Astronaut. 2014 Jan 1;93:366–73.
2. Mishra RS, Ma ZY. Friction stir welding and processing. Mater Sci Eng R Rep. 2005;50(1–2):1–78.
3. Shen J, Wen L, Li Y, Min D. Effects of welding speed on the microstructures and mechanical properties of laser welded AZ61 magnesium alloy joints. Mater Sci Eng A. 2013 Aug 20;578:303–9.
4. Gharacheh MA, Kokabi AH, Daneshi GH, Shalchi B, Sarrafi R. The influence of the ratio of rotational speed/traverse speed (ω/v) on mechanical properties of AZ31 friction stir welds. Int J Mach Tools Manuf. 2006;46(15):1983–1987.
5. Chen J, Fujii H, Sun Y, Morisada Y, Kondoh K, Hashimoto K. Effect of grain size on the microstructure and mechanical properties of friction stir welded non-combustive magnesium alloys. Mater Sci Eng A. 2012 Jul 15;549:176–84.
6. Akinlabi SA. Friction stir welding process: a green technology. World Acad Sci Eng Technol Int J Mech Aerosp Ind Mechatron Manuf Eng. 2012 Jan 1.
7. Johnson R. Friction stir welding of magnesium alloys. InMaterials Sci Forum. 2003 Jul 1;419.

8. Stern A, Munitz A, Kohn G. Application of welding technologies for joining of Mg alloys: Microstructure and mechanical properties. Magnesium Technology. 2003 Jul 21;2003:163–8.
9. Johnson R, Threadgill P. Friction stir welding of magnesium alloys. InEssential Readings in Magnesium Technology. 2016:487–92. Cham: Springer International Publishing.
10. Li N, Pan TY, Cooper RP, Houston DQ, Feng Z, Santella ML. Friction stir welding of magnesium AM60 alloy. Magnesium Technology. 2004:19–23.
11. Munitz A, Cotler C, Stern A, Kohn G. Mechanical properties and microstructure of gas tungsten arc welded magnesium AZ91D plates. Mater Sci Eng A. 2001;302(1):68–73.
12. Lockyer SA, Russel MJ. Mechanical properties of friction stir welds in Magnesium alloys. InInternational Conference on Magnesium Alloys and Their Applications. 2000 Sep 26.
13. Nakata K, Kim YG, Ushio M. Friction stir welding of Mg-Al-Zn alloys. Trans JWRI. 2002;31 (2):141–146.
14. Park SHC, Sato YS, Kokawa H. Microstructural evolution and its effect on Hall-Petch relationship in friction stir welding of thixomolded Mg alloy AZ91D. J Mater Sci. 2003;38(21): 4379–4383.
15. Lee WB, Yeon YM, Jung SB. Joint properties of friction stir welded AZ31B-H24 magnesium alloy. Mater Sci Technol. 2003;19(6):785–790.
16. Esparza JA, Davis WC, Murr LE. Microstructure-property studies in friction-stir welded thixomolded magnesium alloy AM60. J Mater Sci. 2003;38(5):941–952.
17. Choi DH, Kim SK, Jung SB. The microstructures and mechanical properties of friction stir welded AZ31 with CaO Mg alloys. J Alloys Compd. 2013 Mar 25;554:162–8.
18. Suhuddin UFHR, Mironov S, Sato YS, Kokawa H, Lee CW. Grain structure evolution during friction-stir welding of AZ31 magnesium alloy. Acta Mater. 2009;57(18):5406–5418.
19. Zhang D, Suzuki M, Maruyama K. Microstructural evolution of a heat-resistant magnesium alloy due to friction stir welding. Scr Mater. 2005;52(9):899–03.
20. Nagasawa T, Otsuka M, Yokota T, Ueki T. Structure and mechanical properties of friction stir weld joints of magnesium alloy AZ31. In: Essential Readings in Magnesium Technology. Cham: Springer; 2016. p. 517–521.
21. Afrin N, Chen DL, Cao X, Jahazi M. Microstructure and tensile properties of friction stir welded AZ31B magnesium alloy. Mater Sci Eng A. 2008;472(1–2):179–186.
22. Lee WB, Kim JW, Yeon YM, Jung SB. The joint characteristics of friction stir welded AZ91D magnesium alloy. Mater Trans. 2003;44(5):917–923.
23. Mishra RS, Mahoney MW. Friction stir processing: a new grain refinement technique to achieve high strain rate superplasticity in commercial alloys. InMaterials Sci Forum. 2001 Jan 15;357:507–14. Trans Tech Publications Ltd.
24. Hu CM, Lai CM, Du XH, Ho NJ, Huang JC. Enhanced tensile plasticity in ultrafine-grained metallic composite fabricated by friction stir process. Scr Mater. 2008;59(11):1163–1166.
25. Lee WB, Lee CY, Kim MK, Yoon JI, Kim YJ, Yeon YM, et al. Microstructures and wear property of friction stir welded AZ91 Mg/SiC particle reinforced composite. Compos Sci Technol. 2006;66(11–12):1513–1520.
26. Elangovan K, Balasubramanian V. Influences of pin profile and rotational speed of the tool on the formation of friction stir processing zone in AA2219 aluminium alloy. Mater Sci Eng A. 2007;459(1–2):7–18.
27. Azizieh M, Kokabi AH, Abachi P. Effect of rotational speed and probe profile on microstructure and hardness of AZ31/Al_2O_3 nanocomposites fabricated by friction stir processing. Mater Des. 2011;32(4):2034–2041.
28. Balakrishnan M, Dinaharan I, Palanivel R, Sivaprakasam R. Synthesize of AZ31/TiC magnesium matrix composites using friction stir processing. J Magnes Alloys. 2015;3(1):76–78.
29. Faraji G, Dastani O, Mousavi SA. Microstructures and mechanical properties of Al_2O_3/AZ91 surface nanocomposite layer produced by friction stir processing. Proc Inst Mech Eng B J Eng Manuf. 2011;225(8):1331–1345.

30. Khayyamin D, Mostafapour A, Keshmiri R. The effect of process parameters on microstructural characteristics of AZ91/SiO_2 composite fabricated by FSP. Mater Sci Eng A. 2013;559:217–221.
31. Asadi P, Besharati Givi MK, Faraji G. Producing ultrafine-grained AZ91 from as-cast AZ91 by FSP. Mater Manuf Process. 2010;25(11):1219–1226.
32. Mehra D, Mahapatra MM, Harsha SP. Processing of RZ5-10 wt.% TiC in-situ magnesium matrix composite. J Magnes Alloys. 2018;6(1):1–9.
33. Mehra D, Mahapatra M, Harsha SP. Effect of varying wt% of TiC on mechanical and wear properties of RZ5-TiC in-situ composite. Int J Manuf Mater Mech Eng. 2018;8(2):45–56.
34. Mehra D, Mahapatra MM, Harsha SP. Effect of wear parameters on dry abrasive wear of RZ5-TiC in-situ composite. Ind Lubr Tribol. 2018;70(8):1455–1464.

